Research Square

Preprints are preliminary reports that have not undergone peer review.
They should not be considered conclusive, used to inform clinical practice,
or referenced by the media as validated information.

Enantiodivergent Hydroxylation and Recognizable Kinetic of Halocompounds

Yong-Zheng Chen

yzchen@zmu.edu.cn

Zunyi Medical University https://orcid.org/0000-0003-1211-3486

Ting Ma

Zunyi Medical University

Hai-Bo Cui

Zunyi Medical University

Xu Zhang

Zunyi Medical University

Dan Liu

Zunyi Medical University

Yu-Li Yang

Zunyi Medical University

Xue-Qin Ran

Zunyi Medical University

Hua Wan

Zunyi Medical University

Zheng-Yi Tang

Zunyi Medical University

Jie Yang

Zunyi Medical University

Ya Lv

National Key Laboratory of Green Pesticide, Key Laboratory of Green Pesticide and Agricultural Bioengineering, Ministry of Education, Guizhou University

Article

Keywords: P450 monooxygenase, Enantiodivergent Hydroxylation, Recognizable Kinetic, Halohydrins

Posted Date: July 4th, 2025

DOI: https://doi.org/10.21203/rs.3.rs-6645513/v1

License: This work is licensed under a Creative Commons Attribution 4.0 International License.
Read Full License

Additional Declarations: There is **NO** Competing Interest.

Version of Record: A version of this preprint was published at Nature Communications on October 9th, 2026. See the published version at https://doi.org/10.1038/s41467-026-78486-w.

Abstract

Chiral recognition constitutes the central element of asymmetric catalysis. The greater diversity of substituent groups introduced, the more precise control over stereoselectivity becomes. The recognition of high similarity between substituents has been a challenge in asymmetric catalysis. Herein, we report an enzymatic approach enabling kinetically enantioselective hydroxylation in excellent stereoselectivity, though the difference of substituent radius between methyl and chloro substituents is 0.07 Å. Mechanistic investigations involving molecular dynamic simulation and DFT calculation reveal that the engineered P450PL2 exhibits remarkable steric discrimination capability, which enables host-guest interaction with a chiral center bearing methyl and chloro substituents. The biocatalytic system provides efficient access to the 2-chloro-benzyl alcohol derivatives with up to 99:1 enantiomeric ratio and > 99:1 diastereomeric ratio.

Introduction

The essence of asymmetric catalysis is the catalyst's superior ability to discriminate enantiomers based on steric and/or electronic disparities among the substituents of substrates.[1,2] Previous work has focused on substrates with distinct substituents, particularly those with a combination of aryl and alkyl groups. Or introduce oxygen-containing functional groups (e.g., hydroxyl) as "auxiliary analytical groups" to enhance chiral recognition *via* hydrogen-bonding networks or dipole-dipole interactions (Fig. 1A).[2–6] In contrast, the transformation of substrates involving only the subtle stereochemical and/or electronic differences of substituents presents greater difficulties.[7–9] Although recent studies have successfully resolved several sterically similar pairs, including methyl/ethyl and ethyl/*n*-propyl systems (Fig. 1B),[8–14] the stereochemical transformation involving methyl/halogen groups remains unresolved. This difficulty stems from the drastically reduced van der Waals radius difference between methyl -chlorine (Δr_vdW = 0.07 Å) compared to methyl-ethyl systems (Δr_vdW = 0.26 Å).[15] The development of catalytic strategies capable of discriminating systems with subtle stereochemical differences remains a major challenge in asymmetric catalysis.[16–20]

Enzymes have developed a synthetic strategy for precise control of organic transformations through the fine-tuning of their active sites and the synergistic interplay of a series of secondary interactions.[21–23] The amino acid residue network at the active site establishes a chiral microenvironment through hydrogen bonding, electrostatic interaction and van der Waals forces, thus efficiently promoting the catalytic transformation of the substrate.[24,25] Although enzymes have significant advantages in controlling stereoselectivity,[26–28] they face challenges in accurately differentiating substrates with only slight differences in structure.[7,12] Recent studies have shown that the P450 mutant P411-TEA-5274 can efficiently aminate tertiary C-H bonds containing methyl/ethyl racemic tertiary carbon substrates to produce chiral alpha-tertiary amines.[12] This breakthrough highlights that the P450 enzyme catalytic strategy provides a highly promising solution for enantiomeric discrimination in systems with subtle chiral differentiation through directed engineering and dynamic site regulation.

The asymmetric hydroxylation of C-H bonds serves as a highly efficient strategy for constructing chiral alcohols.[29–32] Nevertheless, the hydroxylative synthesis of bis-chiral halohydrins faces challenges due to limited stereochemical discrimination between halogen and methyl groups in racemic substrates and their tendency to form four stereoisomers. Furthermore, precise optimization of enzyme steric bulk is essential to reconcile stereoselectivity demands with the prevention of unfavorable steric interactions at adjacent tertiary sp^3 carbons. These inherent complexities could lead to bifurcated reaction pathways, ultimately yielding enantioenriched products with compromised enantiomeric ratio. Encouraged by our recent findings,[33–36] we herein report the enantio- and diastereoselective hydroxylation reactions catalyzed by engineered P450PL2 in the presence of adjacent tertiary carbon stereocenters (Fig. 1D). In this study, the P450-catalyzed stereoselective hydroxylation process simultaneously controls adjacent stereocenters with substrate selectivity challenges, thereby providing the fastest-reacting stereoisomer halohydrin in the form of enantio- and diastereomerically. We employed diverse mutagenesis strategies to enhance both the substrate and stereoselectivity of P450PL2, achieving enantiodivergent synthesis of double chiral haloalcohols. The engineered variant exhibits superior enantiomeric discrimination toward substituents exhibiting minimal structural variations ($\Delta r_vdW < 0.1$ Å), enabling precise stereoselective control in substrate recognition and hydroxylation reactions. Through an integrative approach combining structural biology and computational modeling, we elucidated how evolutionarily optimized variants modulate protein conformational dynamics to regulate substrate selectivity and stereoselectivity.

Results and discussion

Initial discovery and evolution of P450PL2 monooxygenase

We initiated the study by testing the hydroxylation of (2-chloropropyl)benzene (**1a**, Fig. 2A) by engineered cytochrome P450 collected in the laboratory. A screening of various P450s was conducted, revealing that while most of them were effective in catalyzing the hydroxylation reaction, they did not yield products with high chiral purity (Fig. 2B). The production of high enantiomeric ratio (*er*) and nearly 50:50 diastereomeric ratio (*dr*) by self-sufficient P450 enzymes, such as P450DA and P450DG, implies a lack of selectivity towards the hydroxylation of the **1a** substrate. P450PL2-1 derived from *Parvibaculum lavamentivorans* DS-1 exhibited a difference, with its single-configuration product achieving a 63% proportion. Moreover, the enzyme showed an obvious (*S*)-**1a** preference for hydroxylation. Considering factors such as yield, *er* and *dr* values comprehensively, we believe that P450PL2-1 has greater potential for substrate recognition.

Wild-type P450PL2 (WT) serves as the original point for directed evolution. In order to improve its stereoselectivity, we conducted iterative site-saturation mutagenesis (ISM)[37] followed by screening. To provide more accurate guidance for the modification work, we determined the protein structure of P450PL2 using X-ray crystallography (PDB: 9LW0). Combining molecular docking and related P450PL2 modification literature,[36,38] we selected sites near the heme cofactor (HEME) and substrate binding pocket, as well as the P450 substrate recognition site (SRS),[38,39] for saturation mutagenesis (Fig. 2C).

During the first round of screening, 13 of the 22 amino acid positions demonstrated the presence of mutants exhibiting enhanced stereoselectivity (Supplementary Table 3, Supplementary Fig. 2). In the second round of saturation mutagenesis, we selected the mutant strain P300H with better yield and stereoselectivity (*er* = 97:3, *dr* = 84:16, yield = 25%) as the parent strain, and continued to select the aforementioned candidate sites for subsequent iterative saturation mutagenesis. The *dr* of the product of its next-generation mutant P300H/V99I was increased to 92:8 (Supplementary Table 4), and this was used as the parent strain for the subsequent round of mutation screening. Regrettably, during the third round of mutation screening, we failed to identify any mutants that exhibited a substantial enhancement in either enantioselectivity or diastereoselectivity. Directed evolution has the potential to reach absolute optimality, yet it may also become trapped at a local fitness peak.[40,41] The research by Reetz et al. found that in stereoselective engineering, by using mutants with lower enantioselectivity as templates for subsequent upward climbing, one can escape from local minima.[42,43] To escape the current predicament, we selected the mutant P300L, which had slightly inferior diastereoselectivity compared to P300H, as the template for a new round of engineering. In this round of mutagenesis, we obtained a mutant P300L/L96I with significantly improved *dr* to 94:6 (Fig. 2D, Supplementary Table 5). Taking into account the cooperative effects of the enzyme active sites,[44,45] we employed the WT as a template and conducted combinatorial codon mutagenesis (CCM) on residues with substantial influence on stereoselectivity, thereby establishing a diverse mutant library.[46] After screening, some mutants with improved enantioselectivity and diastereoselectivity were obtained, but their catalytic selectivity did not reach the level of P300L/L96I. Notably, the enzyme's enantioselectivity towards the formation of **1a** was improved significantly during the semi-rational evolution campaign, increasing from 73.5:26.5 *er* (P450PL2-WT, Fig. 2D) to 98:2 *er* (P450PL2-P300L/L96I, Fig. 2D). Additionally, the diastereoselectivity was substantially elevated to 94:6.

Reversing the enantioselectivity and substrate selectivity of P450PL2 monooxygenase

The pursuit of enantiodivergent biocatalytic reactions represents an intriguing and formidable endeavor.[47,48] Numerous enzymes have been optimized to exhibit exceptional stereoselectivity, yet achieving the inversion of an enzyme's enantioselectivity remains a formidable challenge.[49,50] This necessitates intricate remodeling at the active site, coupled with extensive protein engineering efforts to invert the enzyme's enantiomeric preference.[51,52] Particularly when dealing with racemic substrates, achieving the inversion of an enzyme's enantioselectivity poses even greater challenges. In the aforementioned modification work, we noticed that the 303 site located on the loop adjacent to heme has the ability to reverse the enzyme's stereoselectivity (Supplementary Fig. 3), so we decided to try modifying P450PL2 to obtain high-chirality-purity (1*S*, 2*R*)-**2a**. Our initial attempts were challenging, as the saturation mutagenesis results at position 303 revealed that multiple mutants had the ability to reverse stereoselectivity (Supplementary Table 7). We first chose the mutant L303G with the highest yield as the template for mutagenesis. After two rounds of iterative saturation mutagenesis, the *er* of

(1*S*, 2*R*)-**2a** only reached about 80:20, while the yield decreased significantly (Supplementary Table 9). Consequently, we chose another mutant L303P with a higher *er* from the first round as the template for subsequent modifications. Following the second round of iterative saturation mutagenesis, the stereoselectivity still did not show a breakthrough, and the yield decreased significantly (Supplementary Table 10). Considering that the optimal mutants at position 303 did not perform well when combined with other sites, we thought that the 303 site may not be a suitable partner. Therefore, we chose to screen a mutation library with orthogonal combinations of multiple sites. Through numerous screenings, we successfully identified a mutant, L109I/L303S/A253T, that exhibited favorable reversed stereoselectivity and yield (*er* = 94:6, *dr* = 86:14, yield = 15%). Employing various modification techniques and strategies, we ultimately obtained several mutant strains capable of performing dynamic kinetic resolution and benzylic hydroxylation on the substrate, highly stereoselective yielding (1*R*, 2*S*)-**2a** and (1*S*, 2*R*)-**2a** (Fig. 2D, E).

Experimental and computational study

To gain a deeper understanding of the mechanism of this biotransformation, we conducted a series of experiments and computational simulations. Initially, enantiomerically pure substrates (*R*)-**1a** and (*S*)-**1a** were synthesized and subjected to reaction catalyzed by both WT and mutants (Fig. 3A). Experimental results showed that the WT converted (*S*)-**1a** to **2a** with much higher efficiency (780 TTN, Fig. 3A) compared to the conversion of (*R*)-**1a** to **2a** (470 TTN, Fig. 3A), indicating that the enzyme prefers the (*S*)-enantiomer. The mutant P300L/L96I (DS), engineered for enhanced selectivity, demonstrates a hydroxylation efficiency for (*S*)-**1a** that is five times greater than that for *R*-configurations (840 TTN *vs*. 160 TTN, Fig. 3A). This ratio further increases to 12.5 in racemic mixtures (Supplementary Table 20), these evidencing a marked improvement in substrate selectivity for the mutant. In addition, we also noted that the hydroxylation stereoselectivity of this mutant for (*R*)-**1a** has flipped from the *S*-configuration preference of the WT to an *R*-configuration preference. The P450PL2 mutant L109I/L303S/A253T (DR), featuring a reversed stereoselectivity, exhibits a conversion rate for (*S*)-**1a** that is approximately one half of that for (*R*)-**1a** (60 TTN *vs*. 110 TTN, Fig. 3A). In the context of racemic substrates, this disparity translates to a ratio of approximately 1/5 (Supplementary Table 20). Furthermore, our experiments have confirmed that the hydroxylation of **1a** preserves the chiral chlorine configuration of the substrate, without altering the chirality of the chlorine atom during the process. Consequently, the foundation for the P450PL2 mutant to accomplish highly enantioselective and diastereoselective synthesis of **2a** rests on its ability to perform stereoselective hydroxylation within the kinetic resolution of racemic **1a**.

In order to further understand this nearly symmetric enantioselectivity resolution reaction, we sought to explore the transition state barrier for competing hydroxylation reactions using DFT methods. As shown in Fig. 3C, the C − H abstraction barrier for the (*R*)-**1a** benzyl C − H bond (pro-*R* hydrogen and pro-*S* hydrogen) hydroxylation respectively is 25.5 kcal/mol and 21.8 kcal/mol. The computed C − H abstraction barriers for (*S*)-**1a** are 22.0 kcal/mol and 25.6 kcal/mol for the pro-*R* and pro-*S* hydrogens,

respectively. These computational results suggest that, for both substrates, the generation of *anti*-**2a** exhibits a lower C – H abstraction barrier than the *syn*-**2a**. This offers a partial explanation for the preferential production of *anti*-**2a** by both the WT and mutant variants of P450PL2. Regarding the kinetic resolution hydroxylation of the substrate, DFT calculations alone cannot elucidate the preference, as the C – H abstraction barriers for generating *anti*-**2a** from the two substrate conformations are nearly identical (21.8 kcal/mol for (*R*)-**1a**, 22.0 kcal/mol for (*S*)-**1a**). Next, we perform molecular dynamics simulations (MD) for more insights on P450PL2 substrate recognition. For each mutant, we performed multiple long MD simulations (3 × 600 ns) based on the docking poses of (*S*)-**1a** or (*R*)-**1a** at the Cpd I active site.

Based on the MD simulations and the proposed favorable conditions for the active conformations conducive to hydroxylation (Cpd I oxygen to hydroxylated C distance ≤ 3.8 Å, Cpd I oxygen, hydroxylated H, hydroxylated C angle no less than 150°),[53] we set out to explore whether the stereoselectivity tendency presented by the simulation trajectories conforms to the stereoselectivity observed in experiments. As illustrated in Fig. 4A, MD simulations of WT with (*R*)-**1a** show that both the pro-*R* and pro-*S* hydrogen atoms at the benzyl position can achieve favorable conditions for hydroxylation, which to some extent explains the low stereoselectivity observed in the reaction between WT and (*R*)-**1a** in experiments. In simulations involving WT with (*S*)-**1a**, the predominant portion of the regions conducive to hydroxylation is occupied by the pro-*R* hydrogen atom at the benzyl position (Fig. 4B), thus making (*S*)-**1a** more productive towards (1*R*, 2*S*)-**2a**. For DS, in simulations with two enantiomers of **1a**, both the pro-*R* hydrogen atoms at the benzyl position reach proposed satisfactory conditions of active poses for hydroxylation (Fig. 4C, D). The mutant DS, with improved stereoselectivity, constrains the angle of the pro-*S* hydrogen atom at the benzyl position of (*R*)-**1a** to approximately 75°, resulting in the pro-*R* hydrogen atom occupying the predominantly advantageous site for hydroxylation and demonstrating opposite stereoselectivity compared to WT. When **1a** interacts with DR, the picture completely changes (Fig. 4E, F). The conformational population of the benzyl position pro-*S* hydrogen atom in (*R*)-**1a** within DR is more concentrated in the ideal hydroxylation area than that of the pro-*R* hydrogen atom. This results in an increased probability of generating (1*S*, 2*R*)-**2a** in the hydroxylation of (*R*)-**1a** catalyzed by DR, leading to a reversal of stereoselectivity. However, in the MD simulations of DR with (*S*)-**1a**, the conformational populations of benzyl hydrogen are broad, leading to DR exhibiting poor stereoselectivity towards (*S*)-**1a**. In conclusion, the simulated conformational distribution results presented above can elucidate the stereoselectivity tendencies of WT and mutants towards the two isomers of **1a** to some extent.

Subsequently, the computational analysis of binding free energies was conducted by the MM-GBSA method[54,55] to further gain insights into the selective hydroxylation behavior of P450PL2 and its mutant towards different **1a** conformations. The binding free energy difference between (*S*)- and (*R*)-**1a** of DS was − 2.02 kcal/mol, which was higher than that of -0.98 kcal/mol of WT (Fig. 5A). The result exhibits a similar trend to the actually observed discrepancy in substrate selectivity. For DR, the binding free energy difference between (*R*)- and (*S*)-**1a** was − 0.79 kcal/mol, suggesting that (*R*)-**1a** was preferable to

hydroxylation. This finding aligns with the experimental finding that DR demonstrates the opposite substrate selectivity to that of WT. Detailed energy decompositions were obtained through MM-GBSA calculations,[56] we conducted studies of the structural and energetic contributions that underlie these observed differences in binding free energy. Substrate – residue pair interaction calculations (Fig. 5B, D, F) revealed that sites 50, 96, 99, 252, 253, 300, 303, and 403 are among the residues establishing the stabilizing interactions with the substrate in all mutants. Meanwhile, the results of stereoselectivity and non-stereoselectivity for these sites in single-point saturation mutagenesis of WT are relatively scattered (Supplementary Fig. 2), further highlighting their importance for substrate selective binding and stereoselectivity of the reaction. By comparing the substrate-residue pair interactions between the two racemates of **1a**, we found that DS exhibits larger differences compared to WT (particularly at sites 50, 96, and 253). This may imply that larger differences in interaction between different configurations and amino acids favor enzyme recognition of the near-symmetric substrate. The two enantiomers of **1a** exhibit almost completely opposite numerical differences in substrate-residue pair interaction for DR compared to DS. We speculate that DR exhibits an opposite substrate recognition tendency compared to both the WT and DS on the basis of these coadjust interactions.

The majority of mutation sites in either DS or DR are situated within loop regions. Residues in loops near or even far from active sites, exhibit remarkable flexibility and diversity, which can influence substrate recognition and catalysis by undergoing conformational changes.[45,57–59] Specifically, the access of substrates to the active site of P450 enzymes is associated with the structurally agile BC loop and FG loop, with the oscillation of the F helix and G helix facilitating the smooth ingress (egress) of substrates (products) into (from) the enzyme's active site.[60–62] In order to investigate how mutation influences the flexibility of enzymes, we determined the root-mean-square fluctuations (RMSFs) for each residue in the WT and all variants. We observed that both in the WT and mutants, the amino acids within the loop exhibit varied flexibility (or RMSF values) in response to different conformational substrates. More pronounced rigidity was observed at the active site residues of WT binding to (*S*)-**1a** (Fig. 5I, ΔRMSF), with residues at positions 45–60 in the B'C loop region and positions 180–197 in the FG loop region particularly highlighting this feature. When the amino acids at positions 96 and 300 within the loop region are mutated to DS, the residues spanning positions 300–320 in the H loop exhibit increased rigidity, while maintaining the same overall trend (Fig. 5J, ΔRMSF). In MD simulations of DR paired with various conformations of **1a**, a distinctly different scenario emerges (Fig. 5K, ΔRMSF). Firstly, the regions in WT and DS that exhibited rigidity towards (*S*)-**1a** are no longer present in this trend. Secondly, the residues spanning positions 137–146 in the H loop, 269–281 at the rear of the I helix domain, and 382–394 at the leading edge of the G loop exhibit increased flexibility. Given this scenario, we can glimpse the extensive conformational alterations in the protein that DR undergoes to accomplish near-symmetric substrate recognition of opposite configurations and the reversal of hydroxylation stereoselectivity. In particular, the fluctuations in flexibility within loop regions distant from the active site highlight our awareness that residues in these remote loops can exert an influence on substrate recognition and catalysis via conformational alterations, accompanied by the remodeling of the binding pocket. Prior studies have indicated that the optimization of protein dynamic networks and significant epistatic

effects can be ascribed to newly introduced mutations,[63–65] encompassing distant mutations as well.[64,66] Considering all these factors, the changes in the dynamic network of evolutionary enzymes may be influenced by distant mutations such as the one at position 109, along with the remodeling of active sites like 253 and 303, which alter the substrate recognition properties of the enzyme.

Substrate scope investigation and preparative-scale reaction

With the optimal mutant in hand, the performance on various substrates after completing the optimization of conditions was investigated. To our delight, these variants exhibited a broad substrate scope, producing a series of highly enantiomerically pure *anti*-haloalcohols (Fig. 6, 7). Initially, we examined the reactivity of P450PL2 mutants towards alkanes substituted with various halogen atoms (**1a**-**1c**) and observed that these mutants exhibited the highest total turnover number (TTN) with chlorinated alkanes (Fig. 6, 2a, 1200 TTN). When the halogen was substituted with fluorine, the stereoselectivity increased; conversely, substitution with bromine resulted in unsatisfactory stereoselectivity (Fig. 6, 2b, 2c). We observed that **1b** and product **2c** underwent degradation, transforming into other compounds within the enzymatic reaction system (data not shown). This degradation could also be a contributing factor to the yields of both compounds. Substrates (**1d**-**1i**) that possess fluoro-, chloro-, and bromo- at different substitutions on the aromatic ring were tested. These mutants selectively hydroxylate the benzyl site of **1d**-**1i**, smoothly delivering (1*R*, 2*S*)-**2d**-**2i** with highly stereoselective and diastereoselectivity (up to > 99:1 *er*, > 99:1 *dr*). The *meta*-F-substituted substrates can be converted into chiral haloalcohols with a high TTN of 849 (Fig. 6, 2e). In addition, this approach can be extended to the substrates bearing weaker electron-withdrawing groups, including -Cl and -Br, albeit the TTN tends to decrease progressively (Fig. 6, 2g-2i). The position of substituents on the benzene ring has a huge impact on P450s' activity and stereoselectivity.[34,67] In the reaction catalyzed by the P450PL2 mutant, when the substituent is in the *meta*-position, the reaction usually yields a higher productivity and selectivity compared to when it is in the *ortho*- or *para*-positions. Next, we synthesized substrates with electron-donating methyl (**1j**, **1k**) and methoxy groups on the phenyl ring (**1l**-**1m**). The enzyme's activity towards the construction of **2j** dropped to 830 TTN, and the enantioselectivities for (1*R*, 2*S*)-**2k** 95:5 *er* (Fig. 6, 2k). When a methoxy group was introduced at the phenyl ring, the enzyme struggled to convert to synthesize halogenated alcohols (Fig. 6, 2m). Upon extension of the carbon chain, there is a slight decline in both the dr and yield of the product **2n** (Fig. 6). Conversely, when confronted with indane-type substrates **1o**, the mutant is capable of synthesizing (1*R*, 2*S*)-**2o** alcohols with the highest TTN (2130 TTN). Moreover, this biocatalytic system is not only applicable to benzene-type compounds but also to heterocyclic substrates ((1*R*, 2*S*)-**2p**, 96:4 *er*, 86:14 *dr*, 420 TTN).

The scope of substrates that produce inverted configurational products is broadly comparable to the aforementioned types of substrates (Fig. 7). The mutant L109I/L303S/A253S exhibits stereoselectivity in generating the chiral fluoroalcohol (1*S*, 2*R*)-**2b** with > 99:1 *er* and > 99:1 *dr*. However, when confronted with bromine-substituted substrate **1c**, no acceptable inverted mutant with the desired reaction was obtained. Among substrates featuring electron-withdrawing substituents on the benzene ring, the

chloride-substituted substrate exhibited a higher TTN (Fig. 7, 2g, 2h). Fluorine-substituted substrates on the benzene ring **1d**-**1f** uniformly demonstrate favorable reaction efficiencies and stereoselectivities. The mutant L109I/L303P achieved a higher catalytic efficiency for **1i** compared to the mutant P300L (170 TTN *vs*. 80 TTN). When facing substrates **1j**-**1l** substituted with electron-donating groups on the benzene ring, these mutants exhibiting inverted stereoselectivity generally exhibit higher stereoselectivities (Fig. 7, 2j-2l), albeit with lower conversion efficiencies compared to those for previously mentioned substrates. Upon scaling up the reaction to preparative dimensions, eight isolated products were obtained ((1*R*, 2*S*)-**2a** with 22% isolated yield, (1*S*, 2*R*)-**2a** with 15% isolated yield, (1*R*, 2*S*)-**2c** with 19% isolated yield, (1*R*, 2*S*)-**2e** with 27% isolated yield, (1*R*, 2*S*)-**2f** with 16% isolated yield, (1*R*, 2*S*)-**2n** with 17% isolated yield, (1*R*, 2*S*)-**2o** with 50% isolated yield, and (1*R*, 2*S*)-**2p** with 20% isolated yield), maintaining full stereoselectivity throughout. These preparative-scale experiments prove the application potential of the chiral *anti*-haloalcohols investigated in this subject.

Noteworthy, our presently reported enantioselective preparations of optically pure halogenated alcohols have multiple applications in asymmetric synthesis (Fig. 8). For example, the OH group of **2c** can be treated with sodium phenolate to obtain sulfide product **3** in excellent yield without affecting the optical purity. Under alkaline conditions, compound **2c** is readily converted into epoxide **4**, which serves as a key intermediate and plays a crucial role in the synthesis of various important optically pure compounds.[68–70] In addition, the OH group of **2c** can be acylated with Ac_2O to give product **5**, and compound **5** can be transformed to azide product **6** in an excellent yield without erosion of the optical purity. Furthermore, our scheme provides a synthetic platform for drug modification. For example, drug molecules Norethinone (oral contraceptive pill) and Erlotinib (EGFR antagonists) can easily react with azide **6** through a Click reaction to obtain the desired functionalized products **7a** and **7b**.

Conclusions

Cytochrome P450 can be evolved to efficiently recognize near-symmetric substrates by utilizing hydroxylation reactions. This study highlights the potential of P450 enzymes in tackling the challenge of selective oxidative transformations of non-oxygenated substrates with subtle chiral distinctions. By leveraging the stereoselective hydroxylation characteristics of engineered P450PL2, we achieved remarkable enantio- and diastereoselective hydroxylation reactions in the presence of adjacent tertiary carbon stereocenters. Employing diverse mutagenesis strategies, we enhanced both the substrate and stereoselectivity of P450PL2, enabling enantiodivergent synthesis of double chiral haloalcohols. What stands out is that the engineered P450PL2 mutants enable highly selective vicinal hydroxylation reactions of near-symmetric halogen substrate that have so far largely eluded efficient and selective catalysis. Experimental and computational approaches revealed that DS significantly demonstrating enhanced selectivity for (*S*)-**1a**, while the mutant DR exhibits a switch in selectivity to (*R*)-**1a**. DFT calculations suggested lower C – H abstraction barriers for *anti*-product formation, partially explaining preferential production. MD simulations reveal conformational distributions that elucidate observed stereoselectivity tendencies. In addition, we found that mutation-induced conformational changes,

particularly in loop regions, affected substrate recognition and catalysis. The flexibility of loop regions distant from the active site influenced binding pocket remodeling, highlighting the role of dynamic network alterations in enzyme evolution. These findings offer molecular insights into the stereocomplementary regulation and enantioselective differentiation of DS and DR mutants towards the near-symmetric **1a**, and their manipulation of enantioselectivity. Research into the substrate scope has demonstrated the compatibility and wide applicability of this enzymatic recognition across a variety of substrates. Leveraging this work, we hope to expand the catalyst library in the future for asymmetric functionalization of more difficult-to-differentiate substrates.

Methods

Protein expression and enzymatic conversion

P450PL2 and co-expressed with Fdr-Fdx electron transport systems were expressed in strain *Escherichia coli* BL21 (DE3) using the pET-28b(+) and pCDFDuet-1 vector. *E.coli* BL21(DE3) and pET-28b(+) were used as expression host and plasmid respectively. pCDFDuet-1 was used to express coenzyme Fdr-Fdx1. Cultivation of *E. coli* (P450PL2-1) cells was carried out using Terrific Broth (TB) Medium containing 50 μg/mL kanamycin and 50 μg/mL streptomycin. After growing at 37°C to an OD_{600} of 0.6–0.8, isopropyl β-D-1-thiogalactopyranoside (IPTG) was added to the final concentration of 0.1 mM. The culture was incubated at 25°C for another 12–14 h for enyzme expression. Recombinant *E. coli* (P450PL2-1) cells that expressed recombinant P450PL2 were harvested by centrifugation at 9000 rpm at 25°C for 3 min. The freshly prepared *E. coli* (P450PL2-1) cells were resuspended in a reaction buffer solution to a dry cell density (g dcw/L) for performing biotransformation. Add 5 mL of the well-mixed bacterial suspension to a 25 mL stoppered ground-mouth Erlenmeyer flask, followed by the addition of 50 μL of the prepared substrate stock solution (400 mM in DMSO), resulting in a final substrate concentration of 4 mM. The reaction was carried out at 25°C and 250 rpm for 24 hours. After the reaction was completed, vortex the reaction mixture thoroughly and transfer 1 mL to a 2 mL EP tube. Add 1 mL of ethyl acetate containing an internal standard for equal-volume extraction, mix vigorously, then centrifuge at 12,000 rpm and 4°C for 3 minutes to achieve complete phase separation. Collect the upper ethyl acetate layer and transfer it to a 1.5 mL EP tube containing anhydrous Na_2SO_4 to remove residual water. Filter the organic phase through a 0.22 μm micropore filter membrane into a clean HPLC vial for subsequent analysis.

Declarations

Competing interests

The authors declare no competing interests.

Data availability

No data was used for the research described in the article.

Acknowledgement

We are grateful for financial support from the National Natural Science Foundation of China (Nos. 32271537 and 22061049), the Science and Technology Department of Guizhou province (QKHRCPTGCC-2023-003, GHJD-2025-001), and the Science and Technology Department of Zunyi (ZSKRPT2020-5, ZSKH-2018-3, ZSKRPT-2021-5).

Contributions

T.M., H.-B.C. and X.Z. designed the experiments and analysed the data. T.M., H.-B.C., X.Z., D.L., Y.-L.Y., X.-Q.R., H.W. and Z.-Y.T. performed the experiments. H.-B.C., J.Y. and Y.L. participated in writing the manuscript. Y.-Z.C. conceived and supervised the project.

References

1. Wijma, H. J. *et al.* Enantioselective enzymes by computational design and in silico screening. *Angew. Chem. Int. Ed.* **54**, 3726-3730 (2015).
2. Niu, S. T. *et al.* Access to enantioenriched compounds bearing challenging tetrasubstituted stereocenters via kinetic resolution of auxiliary adjacent alcohols. *Nat. Commun.* **12**, 3735 (2021).
3. Kayal, S., Kikuchi, J., Shinagawa, N., Umemiya, S. & Terada, M. Kinetic resolution of racemic tertiary allylic alcohols through SN2' reaction using a chiral bisphosphoric acid/silver(I) salt co-catalyst system. *Chem. Sci.* **13**, 9607-9613 (2022).
4. Zehra, S. T. *et al.* Access to enantioenriched molecules with diverse fluorinated tetrasubstituted stereocenters using hydroxy as a kinetic resolution auxiliary group. *Org. Chem. Front.* **9**, 1040-1047 (2022).
5. Papadopulu, Z., Kazeroonian, N., Irran, E. & Oestreich, M. One out of four: Kinetic resolution of stereoisomeric mixtures of secondary alcohols with a quaternary carbon atom in the β-position by Cu–H-catalyzed enantioselective silylation. *ACS Org. Inorg. Au* **2**, 164-168 (2021).
6. Lin, H., Liu, Y. & Wu, Z.-L. Highly diastereo- and enantio-selective epoxidation of secondary allylic alcohols catalyzed by styrene monooxygenase. *Chem. Commun.* **47**, 2610-2612 (2011).
7. Dou, Z. *et al.* Enhanced stereodivergent evolution of carboxylesterase for efficient kinetic resolution of near-symmetric esters through machine learning. *Nat. Commun.* **15**, 9057 (2024).
8. Zhang, F.-H., Zhang, F.-J., Li, M.-L., Xie, J.-H. & Zhou, Q.-L. Enantioselective hydrogenation of dialkyl ketones. *Nat. Catal.* **3**, 621-627 (2020).
9. Zhou, H. *et al.* Organocatalytic stereoselective cyanosilylation of small ketones. *Nature* **605**, 84-89 (2022).
10. Wang, M. *et al.* Asymmetric hydrogenation of ketimines with minimally different alkyl groups. *Nature* **631**, 556-562 (2024).
11. Peng, T. *et al.* Multienzyme redox system with cofactor regeneration for cyclic deracemization of sulfoxides. *Angew. Chem. Int. Ed.* **61**, e202209272 (2022).

12. Mao, R. *et al.* Biocatalytic, enantioenriched primary amination of tertiary C–H bonds. *Nat. Catal.* **7**, 585-592 (2024).
13. Zhong, F., Li, R., Mai, B. K., Liu, P. & Fu, G. C. Photoinduced copper-catalysed deracemization of alkyl halides. *Nature* **640**, 107-113 (2025).
14. Zhang, Y.-F. *et al.* Asymmetric amination of alkyl radicals with two minimally different alkyl substituents. *Science* **388**, 283-291 (2025).
15. Mantina, M., Chamberlin, A. C., Valero, R., Cramer, C. J. & Truhlar, D. G. Consistent van der waals radii for the whole main group. *J. Phys. Chem. A* **113**, 5806-5812 (2009).
16. Borissov, A. *et al.* Organocatalytic enantioselective desymmetrisation. *Chem. Soc. Rev.* **45**, 5474-5540 (2016).
17. Yasukawa, T., Masuda, R. & Kobayashi, S. Development of heterogeneous catalyst systems for the continuous synthesis of chiral amines via asymmetric hydrogenation. *Nat. Catal.* **2**, 1088-1092 (2019).
18. Bahamonde, A., Al Rifaie, B., Martín-Heras, V., Allen, J. R. & Sigman, M. S. Enantioselective markovnikov addition of carbamates to allylic alcohols for the construction of α-secondary and α-tertiary amines. *J. Am. Chem. Soc.* **141**, 8708-8711 (2019).
19. Xi, Y. *et al.* Application of trimethylgermanyl-substituted bisphosphine ligands with enhanced dispersion interactions to copper-catalyzed hydroboration of disubstituted alkenes. *J. Am. Chem. Soc.* **142**, 18213-18222 (2020).
20. Yang, Y., Shi, S.-L., Niu, D., Liu, P. & Buchwald, S. L. Catalytic asymmetric hydroamination of unactivated internal olefins to aliphatic amines. *Science* **349**, 62-66 (2015).
21. Bell, E. L. *et al.* Biocatalysis. *Nat. Rev. Methods Primers* **1**, 46 (2021).
22. Buller, R. *et al.* From nature to industry: Harnessing enzymes for biocatalysis. *Science* **382**, eadh8615 (2023).
23. Kissman, E. N. *et al.* Expanding chemistry through in vitro and in vivo biocatalysis. *Nature* **631**, 37-48 (2024).
24. O'Connell, A. *et al.* Biocatalysis: Landmark discoveries and applications in chemical synthesis. *Chem. Soc. Rev.* **53**, 2828-2850 (2024).
25. Chen, J., Peng, Q., Peng, X., Zhang, H. & Zeng, H. Probing and manipulating noncovalent interactions in functional polymeric systems. *Chem. Rev.* **122**, 14594-14678 (2022).
26. García-Urdiales, E., Alfonso, I. & Gotor, V. Enantioselective enzymatic desymmetrizations in organic synthesis. *Chem. Rev.* **105**, 313-354 (2004).
27. Gagnon, C. *et al.* Biocatalytic synthesis of planar chiral macrocycles. *Science* **367**, 917-921 (2020).
28. Ma, R. *et al.* Biocatalytic thionation of epoxides for enantioselective synthesis of thiiranes. *Angew. Chem. Int. Ed.* **61**, e202212589 (2022).
29. Qin, Y., Zhu, L. & Luo, S. Organocatalysis in inert C-H bond functionalization. *Chem. Rev.* **117**, 9433-9520 (2017).

30. Zhang, H. *et al.* Site- and enantioselective allylic and propargylic C–H oxidation enabled by copper-based biomimetic catalysis. *Nat. Catal.* **8**, 58-66 (2025).
31. Chen, Y., Tang, W. L., Mou, J. & Li, Z. High-throughput method for determining the enantioselectivity of enzyme-catalyzed hydroxylations based on mass spectrometry. *Angew. Chem. Int. Ed.* **49**, 5278-5283 (2010).
32. Yang, Y., Liu, J. & Li, Z. Engineering of P450pyr hydroxylase for the highly regio- and enantioselective subterminal hydroxylation of alkanes. *Angew. Chem. Int. Ed.* **53**, 3120-3124 (2014).
33. Cui, H.-B. *et al.* Cascade bio-hydroxylation and dehalogenation for one-pot enantioselective synthesis of optically active β-halohydrins from halohydrocarbons. *Green Chem.* **21**, 4324-4328 (2019).
34. Cui, H.-B. *et al.* Biocatalytic synthesis of chiral benzylic alcohols via enantioselective hydroxylation by a self-sufficient cytochrome P450 from *Deinococcus gobiensis*. *Synthesis* **56**, 567-572 (2023).
35. Zhou, X.-J. *et al.* Enantiodivergent synthesis of halohydrins by engineering P450DA monooxygenases. *ACS Catal.* **13**, 15948-15955 (2023).
36. Zhang, R.-Y. *et al.* Biocatalytic hydroxylation tertiary C-H bonds for synthesis of chiral tertiary alcohols by cytochrome P450. *Mol. Catal.* **553**, 113791 (2024).
37. Reetz, M. T. & Carballeira, J. D. Iterative saturation mutagenesis (ISM) for rapid directed evolution of functional enzymes. *Nat. Protoc.* **2**, 891-903 (2007).
38. Wang, J. *et al.* Combined photoredox/engineered P450 enzymatic direct dioxygen-functionalization of arylalkanes to chiral acyloins. *Org. Biomol. Chem.* **20**, 9085-9092 (2022).
39. Whitehouse, C. J., Bell, S. G. & Wong, L. L. P450(BM3) (CYP102A1): Connecting the dots. *Chem. Soc. Rev.* **41**, 1218-1260 (2012).
40. Yang, K. K., Wu, Z. & Arnold, F. H. Machine-learning-guided directed evolution for protein engineering. *Nat. Methods* **16**, 687-694 (2019).
41. Packer, M. S. & Liu, D. R. Methods for the directed evolution of proteins. *Nat. Rev. Genet.* **16**, 379-394 (2015).
42. Qu, G., Li, A., Acevedo-Rocha, C. G., Sun, Z. & Reetz, M. T. The crucial role of methodology development in directed evolution of selective enzymes. *Angew. Chem. Int. Ed.* **59**, 13204-13231 (2020).
43. Gumulya, Y., Sanchis, J. & Reetz, M. T. Many pathways in laboratory evolution can lead to improved enzymes: How to escape from local minima. *ChemBioChem* **13**, 1060-1066 (2012).
44. Zhang, Z. G., Lonsdale, R., Sanchis, J. & Reetz, M. T. Extreme synergistic mutational effects in the directed evolution of a baeyer-villiger monooxygenase as catalyst for asymmetric sulfoxidation. *J. Am. Chem. Soc.* **136**, 17262-17272 (2014).
45. Fröhlich, C. *et al.* Epistasis arises from shifting the rate-limiting step during enzyme evolution of a β-lactamase. *Nat. Catal.* **7**, 499-509 (2024).

46. Belsare, K. D. *et al.* A simple combinatorial codon mutagenesis method for targeted protein engineering. *ACS Synth. Biol.* **6**, 416-420 (2017).
47. Sun, S.-Z. *et al.* Enantioselective decarboxylative alkylation using synergistic photoenzymatic catalysis. *Nat. Catal.* **7**, 35-42 (2023).
48. Ju, S. Y. *et al.* Stereodivergent photobiocatalytic radical cyclization through the repurposing and directed evolution of fatty acid photodecarboxylases. *Nat. Chem.* **16**, 1339-1347 (2024).
49. Zhang, J., Huang, X., Zhang, R. K. & Arnold, F. H. Enantiodivergent α-amino C–H fluoroalkylation catalyzed by engineered cytochrome P450s. *J. Am. Chem. Soc.* **141**, 9798-9802 (2019).
50. Calvó-Tusell, C., Liu, Z., Chen, K., Arnold, F. H. & Garcia-Borràs, M. Reversing the enantioselectivity of enzymatic carbene N–H insertion through mechanism-guided protein engineering**. *Angew. Chem. Int. Ed.* **62**, e202303879 (2023).
51. Gomez de Santos, P. *et al.* Repertoire of computationally designed peroxygenases for enantiodivergent C–H oxyfunctionalization reactions. *J. Am. Chem. Soc.* **145**, 3443-3453 (2023).
52. Li, J.-J. *et al.* P450DA monooxygenase-catalyzed chemoselective and enantiodivergent epoxidation of unactivated alkenes. *ACS Catal.* **14**, 16175-16183 (2024).
53. Peng, Y. Q. *et al.* A chemoenzymatic strategy for the synthesis of steroid drugs enabled by P450 monooxygenase-mediated steroidal core modification. *ACS Catal.* **12**, 2907-2914 (2022).
54. Hou, T., Wang, J., Li, Y. & Wang, W. Assessing the performance of the MM/PBSA and MM/GBSA methods. 1. The accuracy of binding free energy calculations based on molecular dynamics simulations. *J. Chem. Inf. Model.* **51**, 69-82 (2010).
55. Wang, E. *et al.* End-point binding free energy calculation with MM/PBSA and MM/GBSA: Strategies and applications in drug design. *Chem. Rev.* **119**, 9478-9508 (2019).
56. Miller, B. R. *et al.* MMPBSA.Py: An efficient program for end-state free energy calculations. *J. Chem. Theory Comput.* **8**, 3314-3321 (2012).
57. Kan, S. B. J., Lewis, R. D., Chen, K. & Arnold, F. H. Directed evolution of cytochrome c for carbon–silicon bond formation: Bringing silicon to life. *Science* **354**, 1048-1051 (2016).
58. Han, Y.-B. *et al.* Structural insights into the broad substrate specificity of a novel endoglycoceramidase i belonging to a new subfamily of GH5 glycosidases. *J. Biol. Chem.* **292**, 4789-4800 (2017).
59. Qu, G. *et al.* Unlocking the stereoselectivity and substrate acceptance of enzymes: Proline-induced loop engineering test. *Angew. Chem. Int. Ed.* **61**, e202110793 (2021).
60. Halpert, J. R. *et al.* Structure-function of cytochromes P450 and flavin-containing monooxygenases: Implications for drug metabolism. *Drug Metab. Dispos.* **26**, 1223-1231 (1998).
61. Gergel, S. *et al.* Engineered cytochrome P450 for direct arylalkene-to-ketone oxidation via highly reactive carbocation intermediates. *Nat. Catal.* **6**, 606-617 (2023).
62. Dodani, S. C. *et al.* Discovery of a regioselectivity switch in nitrating P450s guided by molecular dynamics simulations and markov models. *Nat. Chem.* **8**, 419-425 (2016).

63. Acevedo-Rocha, C. G. *et al.* Pervasive cooperative mutational effects on multiple catalytic enzyme traits emerge via long-range conformational dynamics. *Nat. Commun.* **12**, 1621 (2021).
64. Maria-Solano, M. A., Iglesias-Fernández, J. & Osuna, S. Deciphering the allosterically driven conformational ensemble in tryptophan synthase evolution. *J. Am. Chem. Soc.* **141**, 13049-13056 (2019).
65. Bunzel, H. A. *et al.* Evolution of dynamical networks enhances catalysis in a designer enzyme. *Nat. Chem.* **13**, 1017-1022 (2021).
66. Osuna, S. The challenge of predicting distal active site mutations in computational enzyme design. *WIREs Comput. Mol. Sci.* **11**, e1502 (2021).
67. Fu, W. Z. *et al.* A metalloenzyme platform for catalytic asymmetric radical dearomatization. *Nat. Chem.* **16**, 1999-2008 (2024).
68. Song, H. *et al.* Activation of epoxides by a cooperative iron–thiolate catalyst: Intermediacy of ferrous alkoxides in catalytic hydroboration. *ACS Catal.* **7**, 7709-7717 (2017).
69. Tiecco, M. *et al.* Synthesis of enantiomerically pure substituted tetrahydrofurans from epoxides and phenylselenium reagents. *Tetrahedron: Asymmetry* **15**, 405-412 (2004).
70. Cresswell, A. J. *et al.* β-fluoroamphetamines via the stereoselective synthesis of benzylic fluorides. *Org. Lett.* **12**, 2936-2939 (2010).

Figures

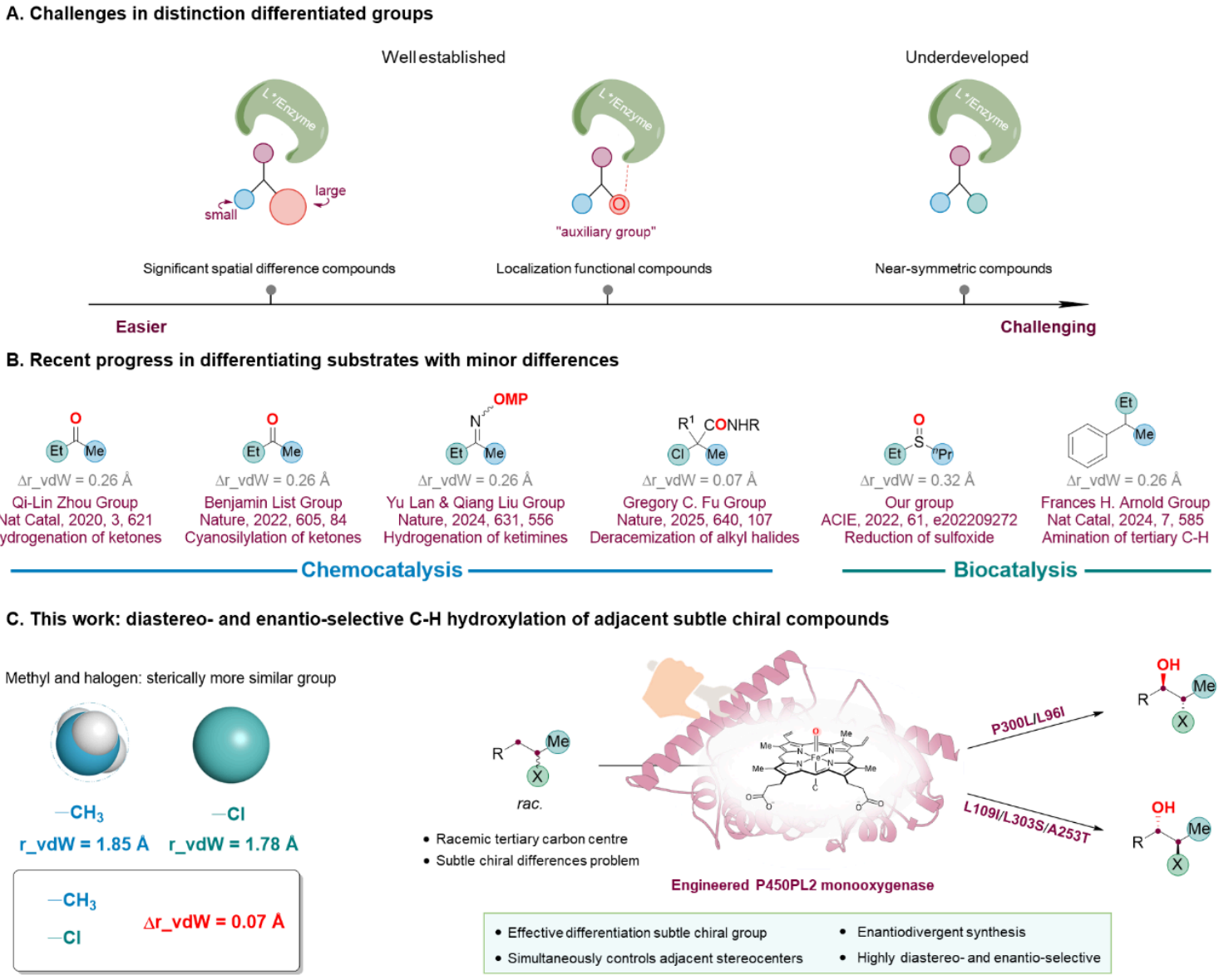


Figure 1

Overview of the chiral recognition in catalytic asymmetric synthesis. A Challenges in distinguishing differentiated groups in asymmetric synthesis. **B** Recent progress in differentiating substrates with minor differences. **C**Diastereo- and enantio-selective C-H hydroxylation of adjacent subtle chiral tertiary carbon centre compounds in this work.

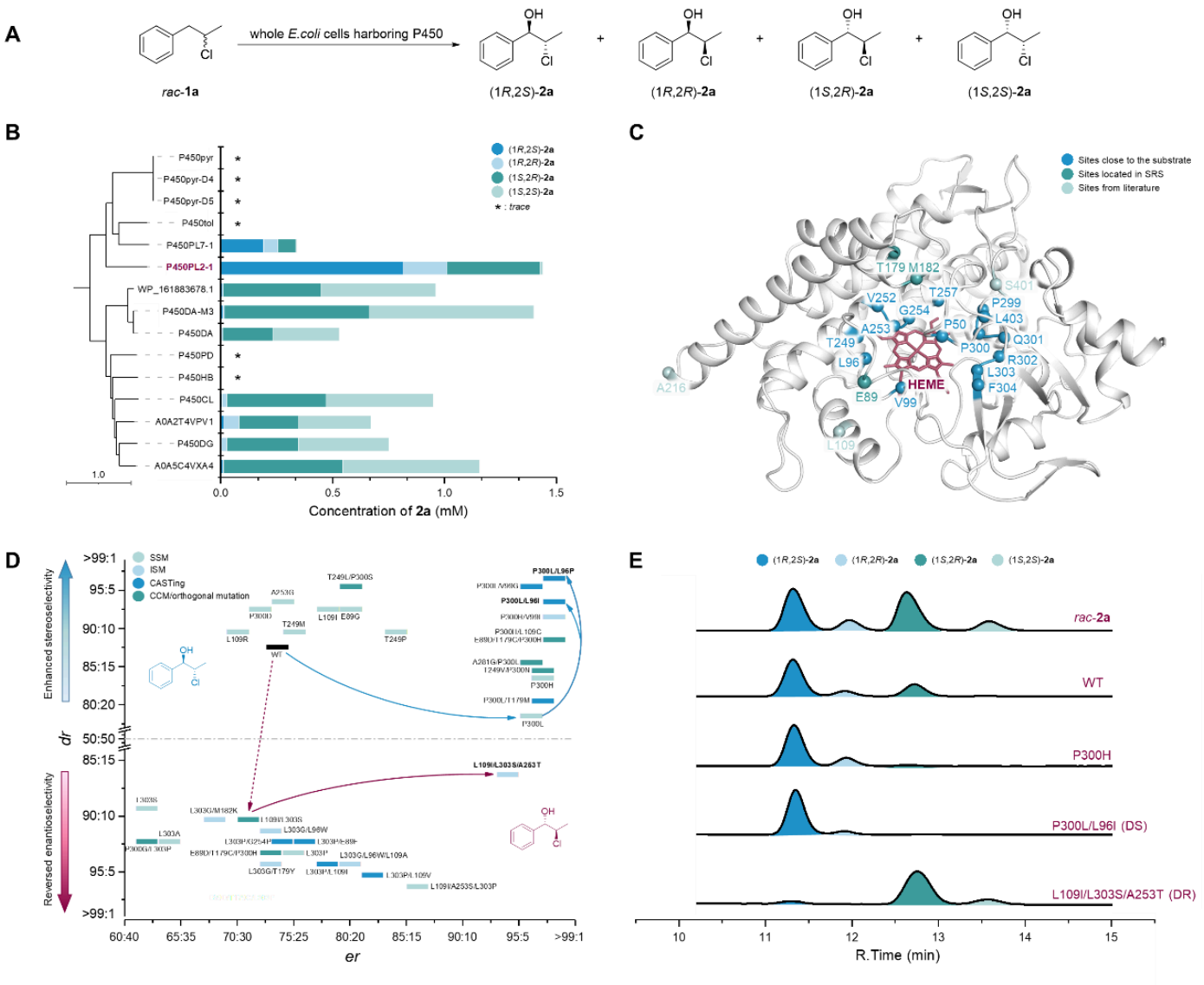


Figure 2

Identification and directed evolution of P450PL2. A Enantioselective hydroxylation and divergent kinetics of (*rac*)-**1a**by P450s. **B** Enzymes are screened for enantioselective hydroxylation and divergent kinetics of (*rac*)-**1a**. **C** Mutated amino acid positions in cytochrome P450PL2. **D** Directed evolution strategies and approaches of P450PL2. **E** HPLC chromatograms of the catalytic results of wild-type and different mutants.

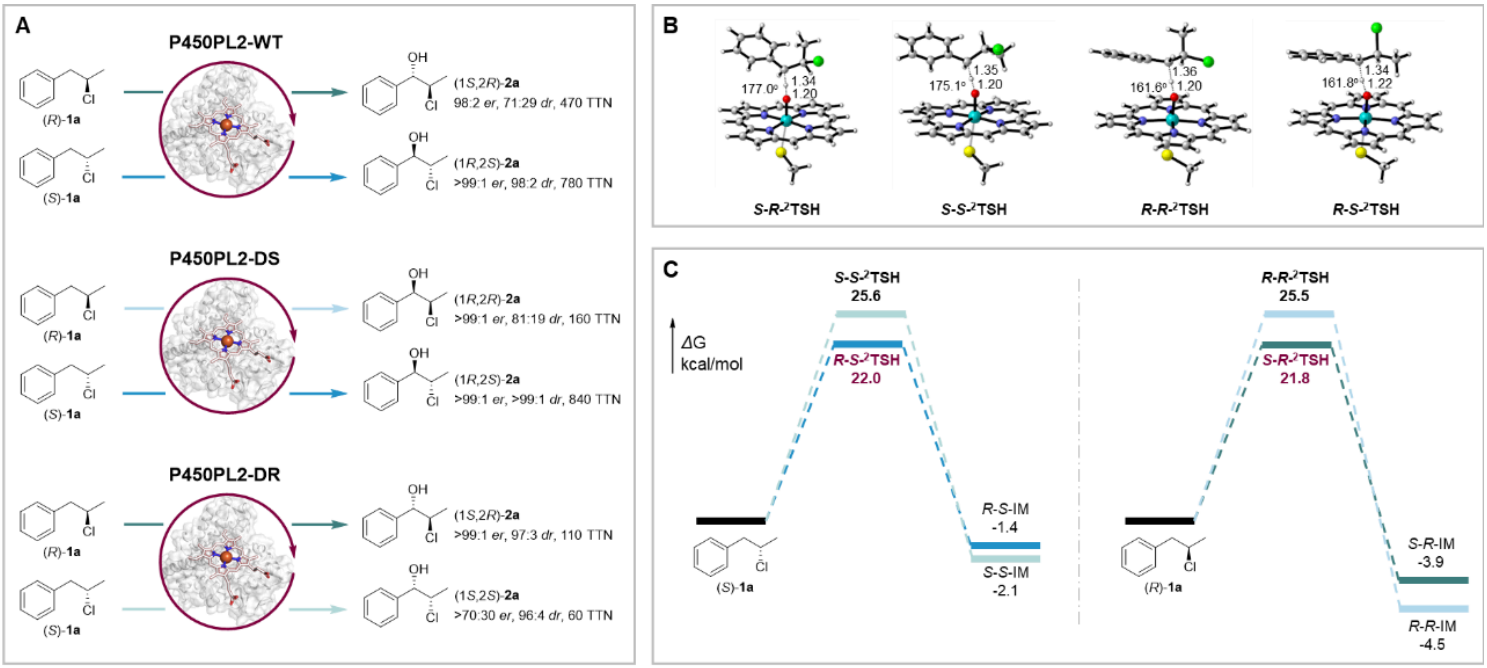


Figure 3

Mechanistic Studies of the Reaction. A Enzymatic reactions of enantiomerically pure substrates (*R*)-**1a**and (*S*)-**1a** with P450PL2 and mutants. **B** Possible transition state postures of four configurational products. **C** C–H abstraction barrier for four configurational products. TTN is defined as the (molar) amount of indicated product divided by the amount of haem protein in the reaction, as measured by the CO-difference spectral assay (see Supplementary 1.7 for more details).

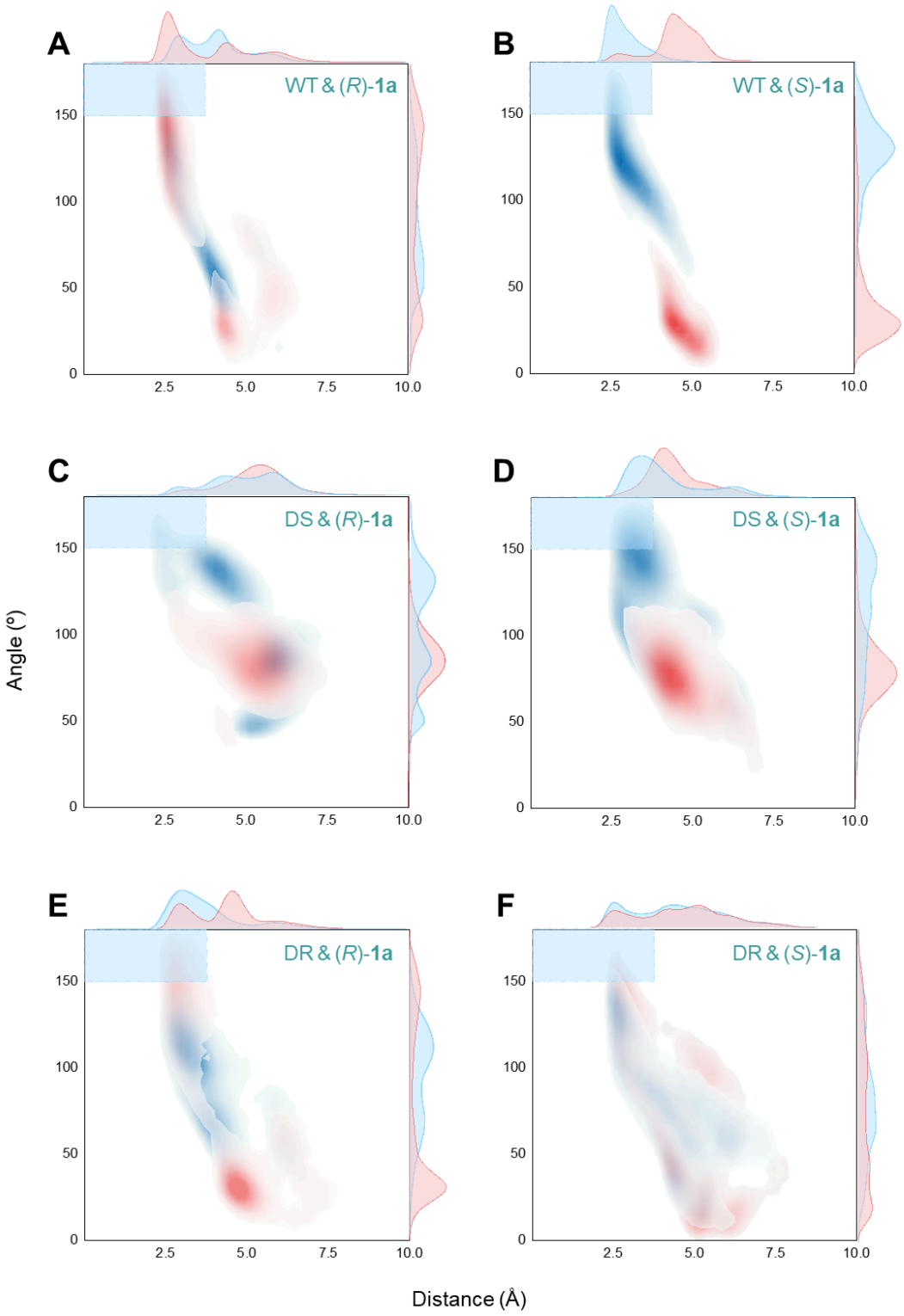


Figure 4

Conformational population analysis of key geometric parameters for hydroxylation of P450PL2 and mutants with two enantiomers of 1a. **A-F** Molecular dynamics simulation of P450PL2-WT/(*R*)−**1a**, P450PL2-WT/(*S*)−**1a**, P450PL2-DS/(*R*)−**1a**, P450PL2-DS/(*S*)−**1a**, P450PL2-DR/(*R*)−**1a**, P450PL2-DR/(*S*)−**1a**. Distances determined between the oxygen atom of haem-Fe=O and the C-atom that have been hydroxylated of **1a** (x-axis) and angles formed by O(Fe=O) – H-atom that have been hydroxylated of **1a** –

C-atom that have been hydroxylated of **1a**(y-axis) from the first replica of the MD dataset. The pro-*R* hydrogen at the benzyl position of **1a** is shown in blue, and the pro-*S* hydrogen is shown in red. The gray field indicates satisfactory conditions of active poses showing both the distance ≤ 3.8 Å and the angle ≥150°.

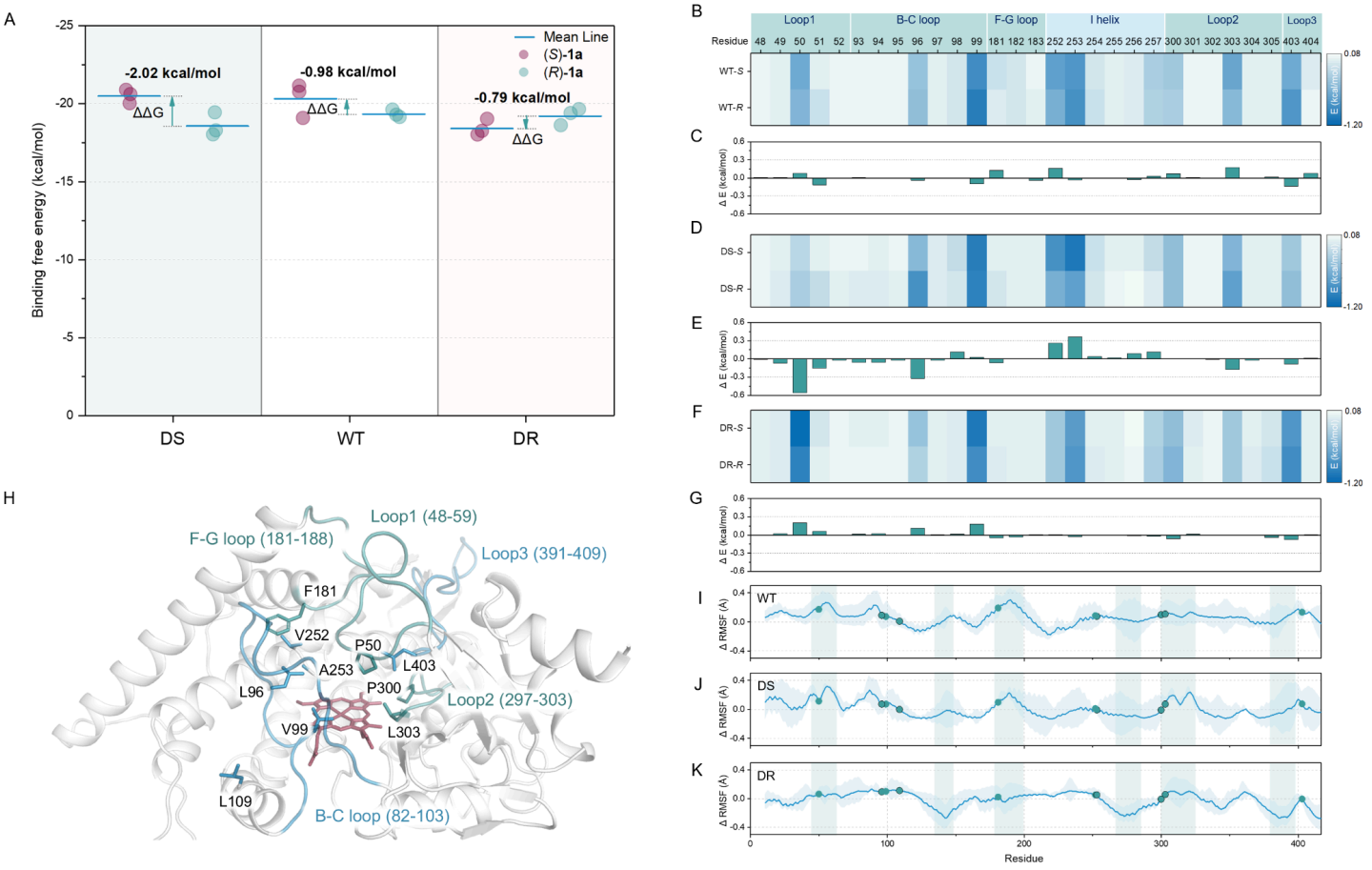


Figure 5

Effect of mutation on enzyme flexibility. A Binding free energy difference of P450PL2 and mutants to substrates of (*R*)-**1a** and (*S*)-**1a**. **B-G** Binding free energy of P450PL2 and mutants to substrates of (*R*)-**1a** and (*S*)-**1a**. **H** Impact of P450 loop regions on catalytic activity. **I-K** The ΔRMSFs for each residue in the WT and mutants.

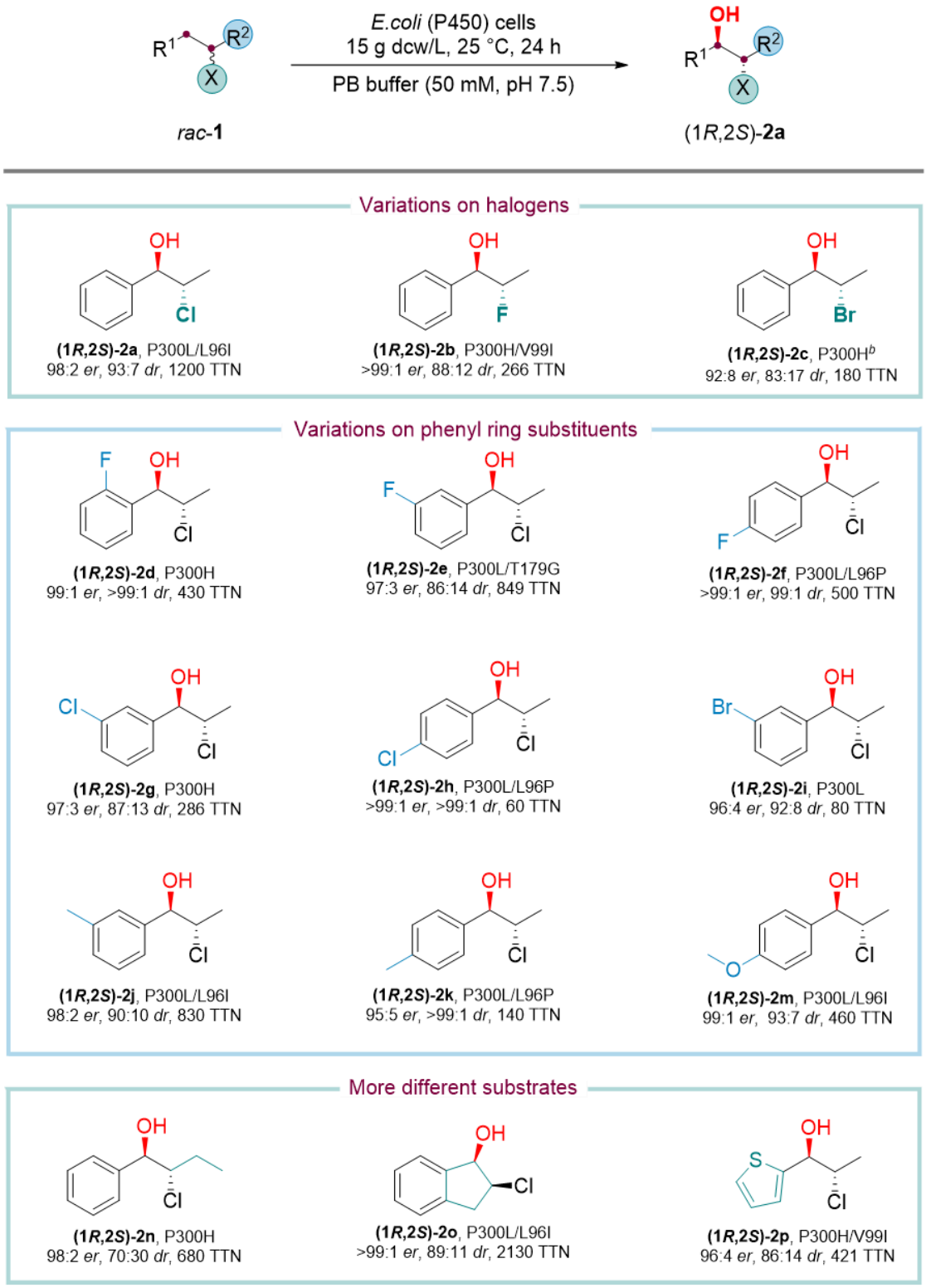


Figure 6

Scope of the biocatalytic enantioselective synthesis of (1*R*, 2*S*)-2.

Reaction conditions: 5 mL PB buffer (50 mM, pH 7.5), 15 g dcw/L *E. coli* (P450PL2 mutants) cells, 4 mM substrates at 25 °C. The yields, *er* and *dr* values were determined by chiral HPLC. [b] The reaction time of **1c** is 1 h.

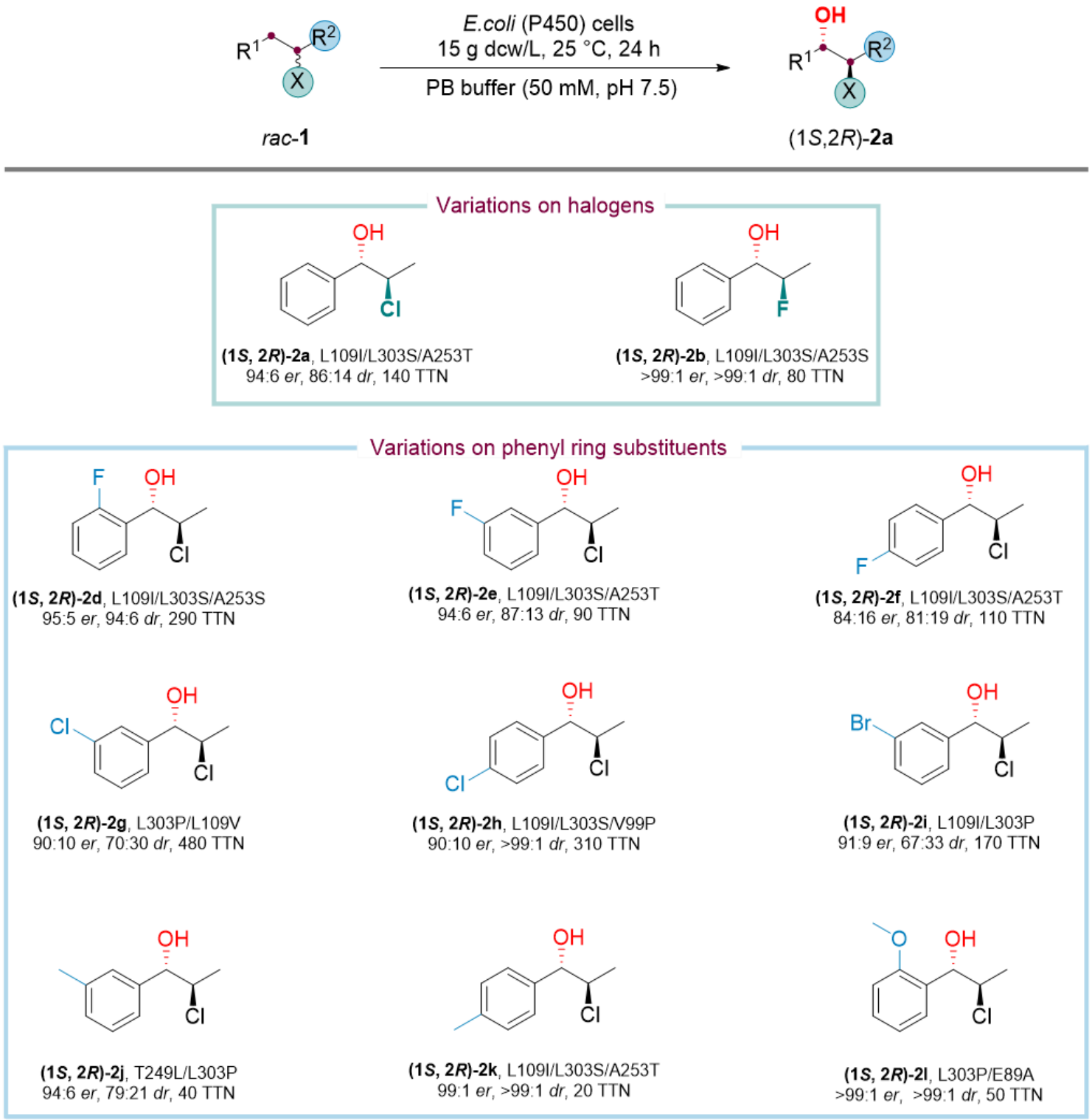


Figure 7

Scope of the biocatalytic enantioselective synthesis of (1*S*, 2*R*)-2.

Reaction conditions: 5 mL PB buffer (50 mM, pH 7.5), 15 g dcw/L *E. coli* (P450PL2 mutants) cells, 4 mM substrates at 25 °C. The yields, *er* and *dr* values were determined by chiral HPLC.

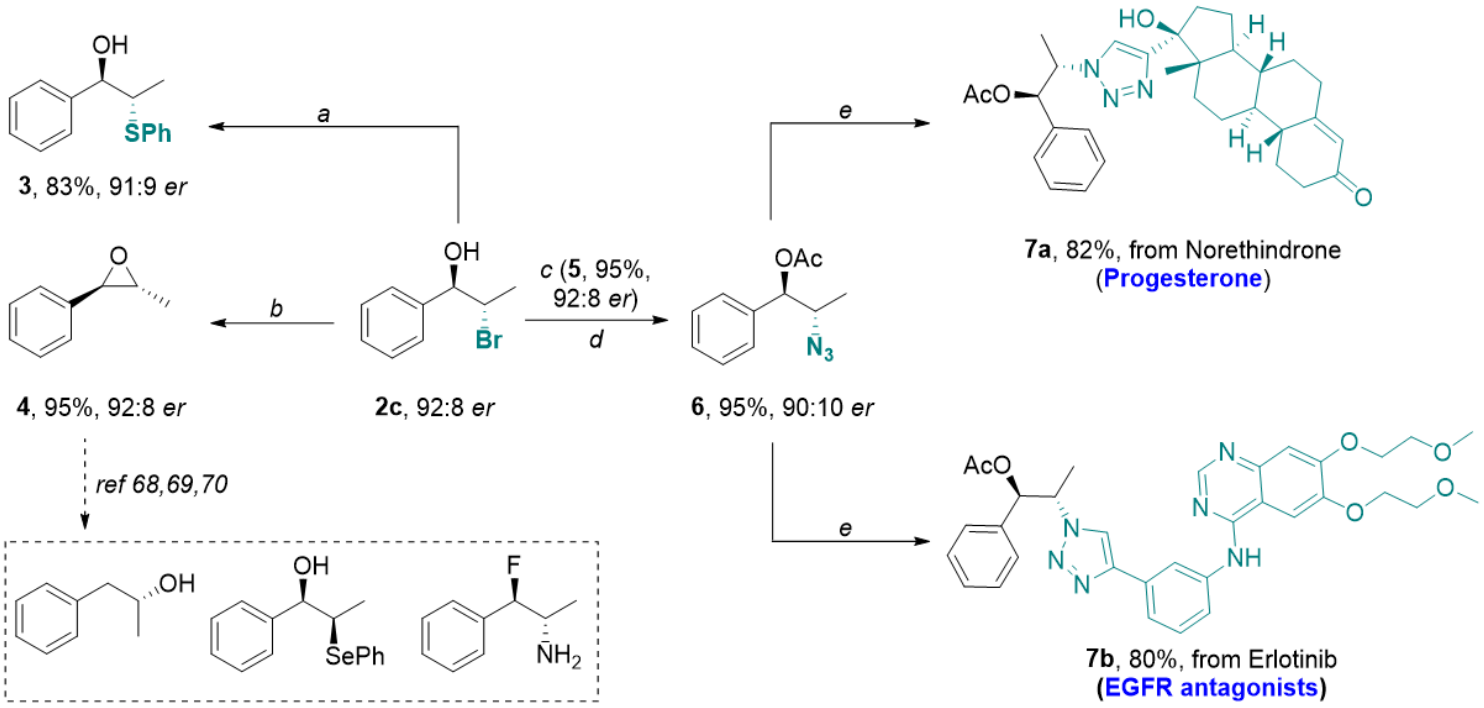


Figure 8

Synthetic transformations of (1*R*, 2*S*)-2c.

Reaction conditions: [a] Sodium thiophenolate, CH_3CN, 25 °C, 3 h; [b] DBU, DCM, 25 °C, 3 h; [c] Ac_2O, Et_3N, DMAP, CH_2Cl_2, 0 °C to r.t., 3 h; [d] NaN_3, DMSO, 80 °C, 6 h; [e] $CuSO_4$, sodium ascorbate, MonoPhos, EtOH/H_2O (v/v = 3/1), Norethindrone or Erlotinib, 70 °C, 6 h.

Supplementary Files

This is a list of supplementary files associated with this preprint. Click to download.

- SupplementaryInformation.pdf